THE ASTROPHYSICAL JOURNAL, 448:611–622, 1995 August 1

HIGH SPATIAL RESOLUTION FABRY-PEROT IMAGING OF M82: NEAR-INFRARED RECOMBINATION LINE OBSERVATIONS

SHOBITA SATYAPAL, DAN M. WATSON,[1] JUDITH L. PIPHER, WILLIAM J. FORREST, DIANA COPPENBARGER, S. NICHOLAS RAINES, SCOTT LIBONATE, AND FRANÇOIS PICHÉ[2]
Department of Physics and Astronomy and C. E. K. Mees Observatory, University of Rochester, Rochester, NY 14627-0171
MATTHEW A. GREENHOUSE AND HOWARD A. SMITH
National Air and Space Museum, Laboratory for Astrophysics, Smithsonian Institution, Washington, DC 20560
KEITH L. THOMPSON[3] AND JACQUELINE FISCHER
Naval Research Laboratory, Remote Sensing Division, Washington, DC 20375-5351
AND
CHARLES E. WOODWARD[4] AND TRACY HODGE
Department of Physics and Astronomy and Wyoming Infrared Observatory, University of Wyoming, Laramie, WY 82071
Received 1994 October 18; accepted 1995 February 10

ABSTRACT

We present high spatial resolution ($\sim 1''$) and moderate spectral resolution ($\lambda/\Delta\lambda \simeq 800$) Pa$\beta$ and Brγ Fabry-Perot imaging observations of the central kiloparsec of M82. These observations, in conjunction with new near-infrared broadband imaging observations, are used to examine the extinction toward the starburst region, the state of the ionized gas, and the nature of the stellar population.

Enhancements in the extinction-sensitive Paβ/Brγ flux ratio are found to trace out the molecular lobes seen in CO, supporting the assumption that we are observing a dense torus surrounding the central stellar clusters and H II regions. Using a nonuniform foreground screen model for the Paβ/Brγ flux ratio, the derived extinction toward the starburst region is found to vary from $A_V \simeq 2$ to $A_V \simeq 12$ mag, significantly smaller than is adopted in most other studies of the stellar population in the starburst region of M82. The extinction-corrected K-magnitude in a 30″ aperture centered on the nucleus is found to be $M_K = -22.0$. This is substantially fainter than previous values adopted, amounting to as much as a reduction of a factor of ~ 3 in the intrinsic K luminosity, a difference that substantially weakens the arguments made previously for a low mass-deficient IMF for the starburst region of M82.

Our recombination line images were used to estimate separately the contribution to the near-infrared continuum bandpasses from free-free and free-bound processes and the emission from dust. These sources of emission do not contribute appreciably to the total near-infrared continuum and thus it can confidently be assumed that this emission is dominated by starlight.

In addition, we present narrow-band imaging observations of M82 in the 3.29 μm unidentified dust feature. The emission is seen to be well-correlated with the Brγ emission. The ratio of the extinction-corrected 3.29 μm dust feature flux to extinction-corrected Brγ flux is found to vary from 4.5 to 15 throughout most of the starburst region, with values greater than 35 near the dynamical center of the galaxy. This variation, along with other star formation diagnostics, suggests that the nucleus contains a later-type stellar population and the starburst phenomena is propagating outward. The ratio of the total far-infrared luminosity to the dereddened 3.29 μm feature luminosity is found to be 1340 ± 260 for M82, significantly smaller than the ratio obtained using the uncorrected 3.29 μm feature flux (1690 ± 200).

Subject headings: galaxies: individual (M82) galaxies: ISM — galaxies: nuclei — infrared: galaxies — infrared: ISM: lines and bands

1. INTRODUCTION

Many galaxies have exhibited signs of extremely active star formation within their nuclear regions. M82, at a distance of 3.2 Mpc, has served as an archetype "starburst" galaxy, having been studied in detail over a wide range of wavelengths. The central kiloparsec of this galaxy is marked by a large far-infrared luminosity, a low mass-to-luminosity ratio, and a large complex of supernova remnants. Qualitatively, these features suggest the presence of active star formation, possibly triggered by an interaction with the nearby galaxy M81. Rieke et al. (1980) described the stellar population of the M82 starburst region using a number of constraints such as the ionizing flux from the younger population, the 2 μm luminosity presumably from the evolved stellar population, and the CO $\Delta v = 2$ band head strength. They found an initial mass function (IMF) deficient in stars less massive than 3 $M_\odot$, substantially different from the solar neighborhood IMF. This conclusion is critically dependent on the constraint imposed by the extinction-corrected 2 μm luminosity. If the 2 μm luminosity is due to evolved stars, then any realistic model must produce enough massive stars in the starburst region that

[1] NSF Presidential Young Investigator.
[2] Present address: Institute of Astronomy, Madingley Road, Cambridge, England, UK.
[3] NSF/NRC Postdoctoral Fellow. Present address: Astronomy Department, University of Texas at Austin.
[4] NSF Presidential Faculty Fellow.

would evolve to the supergiant phase within the timescale of the burst without exhausting the total supply of gas within the starburst region. Since the extinction toward the starburst region of M82 is large and nonuniform, the determination of this extinction, and thus the true colors and luminosities of the stellar clusters, has been difficult and uncertain. In the absence of any high spatial resolution, accurate extinction measurements, recent attempts to model the stellar population (e.g., Rieke et al. 1993; Doane & Matthews 1993) have sought to provide further support for the low-mass cutoff without depending critically on the extinction corrections.

In this article, we investigate the extinction toward the starburst region of M82 using high spatial resolution near-infrared hydrogen recombination-line imaging. Recombination-line intensity ratios, along with appropriate assumptions of an extinction law, yield reliable estimates of extinction toward ionized gas, and in the case of the starburst region of M82, this is approximately the same as the extinction toward most of the young stellar clusters formed in the starburst. In addition, we present J (1.23 μm), H (1.65 μm), and K (2.23 μm) broadband imaging observations as well as imaging in the 3.29 μm unidentified dust feature. These observations comprise some of the best probes of the inner regions of M82 and will allow us to gain more insight into starburst models in general.

2. OBSERVATIONS AND DATA REDUCTION

2.1. *Recombination-Line Images*

We observed M82 during 1993 May at the Wyoming Infrared Observatory (WIRO), a 2.34 m telescope controlled by a single 386 PC running a Forth telescope control system in a DOS operating environment (R. D. Gehrz, T. J. Jones, & C. E. Woodward, in preparation). High spatial resolution ($\sim$1.″2) Brγ (2.16 μm) and Paβ (1.28 μm) images were obtained with the University of Rochester's Third Generation Array Camera coupled with the National Air and Space Museum's J/H-band and the Naval Research Laboratory's K-band Fabry-Perot interferometer (FPI) system. The spectral resolution of the FPIs was $R \equiv \lambda/\Delta\lambda \simeq 800$. Cold circular-variable filters (CVFs) provided FPI order isolation. The plate scale was 0.″23 at 1.28 μm and 0.″25 at 2.17 μm. Plate curvature and coating imperfections in the FPIs resulted in systematic, axisymmetric phase shifts across the array. The maximum shift from center to corner was approximately half a resolution element, making it necessary to sample the line profile to correct for these shifts for all substantially extended sources.

Fabry-Perot data cubes consisting of nine images were obtained in each line. Wavelength spacings of $\frac{1}{3}(\lambda/R)$ and $\frac{1}{4}(\lambda/R)$ R were used to sample the Brγ and Paβ lines, respectively. Continuum images were obtained at $\pm 5/3(\lambda/R)$ for the Brγ observations and at $\pm 2(\lambda/R)$ for the Paβ observations. At each wavelength, a sky-object object-sky image sequence at a 100 s integration time per image was recorded. Flat fields were obtained using early morning sky frames at each of the wavelength positions used. All of the images were corrected for the minor nonlinearity effects of the detector, background subtracted by the nearest sky frame and subsequently calibrated. The standard star BS 3888 (F2 IV; $m_K = 2.990$) was used as the calibrator. Alignment and spatial registration of all the images in each of the data sets was carried out using a cross-correlation procedure, using the position of the farthest compact object in the southwest from the nucleus as a reference.

Correction for the FPI plate curvature across the detector array involved using monochromatic flat fields obtained using argon and krypton discharge lamps. These images were used to measure the FPI transmission function at all positions on the array, generating values for the wavelength offsets and the FWHM corresponding to each pixel. The latter parameters were obtained from a nonlinear Lorentzian fit to the observed lamp emission lines for each pixel in the data cube. These calibrations were then applied to the M82 data set to determined the wavelength and FWHM corresponding to each pixel. A nonlinear fit was again applied to the individual pixels in the M82 data set, generating images of the line flux, the peak wavelength, and the continuum. Upon examination of the spectra in the M82 data cubes, it was found that the observed profile in single pixels was no broader than the instrumental profiles, although the line emission is Doppler-shifted across the galaxy. The fitting function was therefore chosen to be a linear offset term plus a Lorentzian with the same FWHM as the instrumental profile. The IRAF/STSDAS[5] software packages were used for all the data reduction. Both the Brγ and Paβ data sets were processed in this manner.

TABLE 1

FILTERS AND VALUES USED FOR BROADBAND PHOTOMETRY

Filter	λ_0 (μm)	$\Delta\lambda_{FWHM}$ (μm)	F_ν (0 mag)(Jy)	Plate Scale[a]	Magnitude of Calibration Star HD 1881
J	1.25	0.29	1632	0.22	7.14
H.....	1.64	0.29	1060	0.23	7.13
K.....	2.16	0.39	684	0.24	7.13

[a] All final images were adjusted to have the same plate scale (0.″47 pixel^{-1}). Units are in arcseconds pixel^{-1}.

2.2. *Near-infrared Broadband and Narrow-Band Images*

The J (1.23 μm), H (1.65 μm), and K (2.23 μm) imaging was carried out in 1992 September at WIRO with the UR Third Generation Array Camera. Four images were taken at 4 s exposures in each of the bandpasses. A cross-correlation routine was used to align the images before co-addition. All images were linearized, background-subtracted, and divided by morning sky flats at the same wavelength. Flux calibration was achieved using the standard HD 18881 ($m_K = 7.140$; Elias et al. 1982). Table 1 summarizes the parameters involved in the broadband observations. The FWHM of the point-spread function was 1.″2.

The 3.3 μm imaging was carried out in 1992 October at WIRO with a 1.85% bandwidth CVF (equivalent width resulting from the convolution of the Gaussian CVF profile with 0.8% resolution and a circular Lyot-stop profile) and the UR Third Generation Array Camera. Images were taken in 32 s exposures at 3.158 μm, 3.291 μm (line center), and 3.376 μm. The data set consisted of 20 on-line frames and 10 off-line frames at each of the continuum settings. Again all images were linearized, background-subtracted, and divided by morning sky flats at the same wavelength. Spatial registration and co-addition was carried out using the same methods that were applied to the broadband data. Since the instrumental width is comparable to the width of the 3.29 μm dust feature, the determination of the feature power involved several assumptions. First, the 3.29 μm feature profile for the inner 2.″6 of M82 from Tokunaga et al. (1991) was assumed to represent the line

[5] STSDAS is distributed by the Space Telescope Science Institute, which is operated by the Association of Universities for Research in Astronomy, Inc., under NASA contract NAS5-26555.

profile of the feature everywhere in the galaxy. The 3.158 μm continuum image was subtracted from the line center image and the result was multiplied by the equivalent width corresponding to the convolution of the instrumental and dust feature widths.

All images of M82 were block-averaged by two pixels in each direction, adjusted for differences in plate scale, and aligned using the cross-correlation routine; the final plate scale of all images is 0".47 pixel^{-1}.

3. RESULTS

At visible wavelengths, M82 is riddled with dark dust lanes, long line-emitting filamentary structures, H II regions, and stellar clusters. The nucleus is obscured at these wavelengths. Figure 1 (and Fig. 2 [Pl. 22]) shows the emission at J, H, K, Brγ, and Paβ. The most distinct feature of the near-infrared images is the bright central concentration. The 2.2 μm emission shows a strong peak at the center of a smooth, symmetric distribution which is seen to be coincident with the dynamical nucleus of the galaxy (Beck et al. 1979). The high and nonuniform extinction is apparent in the differences in morphology in the different bandpasses. The most intense broadband and recombination-line emission is found between the two main peaks seen in CO $J = 1 \rightarrow 0$ and H I 21 cm maps (Lo et al. 1987; Weliachew, Fomalont, & Greisen 1984), suggesting the overall structure of a central starburst cavity containing stellar clusters and relatively low-density ionized gas surrounded by a ring of molecular material, viewed nearly edge-on (Waller, Gurwell, & Tamura 1992). The central cavity contains the 2, 10, 40, 100 μm, and Brγ emission sources, and comprises the main starburst zone (e.g., Telesco et al. 1991). This region consists of stellar clusters, giant H II regions, and a complex of more than 40 radio point sources whose sizes and spectra suggest that they are young remnants of Type II supernovae (Kronberg, Biermann, & Schwab 1985). This central region emits about 4×10^{10} $L_{\odot}$, primarily in the far-infrared. The total dynamical mass within this region is 10^8–10^9 $M_{\odot}$ (Beck et al. 1979).

From our near-infrared observations, we see that the recombination-line emission and the broadband emission are generally not well-correlated. Figure 3 shows the Brγ emission with the K contour plot overlaid. The central few arcseconds are seen to be a strong source of broadband emission, containing little ionized gas compared with the surrounding regions. The Brγ emission is seen to be well correlated with the 3.29 μm unidentified dust feature emission, as shown in Figure 4. The 3.29 μm unidentified dust feature is even better correlated with the 12.4 μm emission (see Telesco & Gezari 1992).

Our recombination-line spectrophotometry is compared with previous measurements in Table 2. Our results are in close agreement with the 3".8 Brγ measurement by Lester et al. (1990) and are within 1.5 σ of the 11" Brγ measurement by Simon, Simon, & Joyce (1979) at the position of "Irb." A large discrepancy is found between our measurements and those of Willner et al. (1977). Willner et al. find a Brγ flux in a 30" beam that is less than the higher spectral resolution 11" Brγ measurement by Simon et al. (1979) at the position of "Irb." However, their Brα flux at the same position is over a factor of 5 times larger than the result of Simon et al. Our Paβ spectrophotometry agrees with the results of Greenhouse et al. (1991) but significant differences exist between our data and the 3" and 6" aperture Paβ measurements by McLeod et al. (1993). We have assessed the accuracy of our spectrophotometry by comparing emission-line fluxes from the bright planetary NGC 7027 with fluxes quoted in the literature. Given the high line-to-continuum ratios and often small spatial extent of bright planetaries,

TABLE 2

SELECTED HYDROGEN RECOMBINATION LINE MEASUREMENTS IN M82

Line	λ (μm)	Aperture Diameter	Position[a]	Observed Flux[b] (10^{-16} W m^{-2})	Reference
Brα	4.051	30	Nucleus	160	Willner et al. 1977
		11	"Ira"	38 ± 3	Simon et al. 1979
		11	"Irb"	30 ± 5	Simon et al. 1979
Brγ	2.167	30	Nucleus	15 ± 7	Willner et al. 1977
		30	Nucleus	53	This paper
		11	"Ira"	7.2 ± 1.7	Simon et al. 1979
		11	"Irb"	17 ± 4	Simon et al. 1979
		11	"Irb"	4.8 ± 0.6	Larkin et al. 1994
		11	"Ira"	14.7	This paper
		11	"Irb"	11.0	This paper
		8	Nucleus	2.2 ± 0.2	Reike et al. 1980
		8	Nucleus	2.5 ± 0.3	Waller et al. 1992
		8	Nucleus	2.6 ± 0.3	Larkin et al. 1994
		8	Nucleus	7.36	This paper
		3.8	Nucleus	2.00 ± 0.04	Lester et al. 1990
		3.8	Nucleus	1.71	This paper
Paβ.....	1.282	3	Nucleus	1.47 ± 0.01	McLeod et al. 1993
		3	Nucleus	3.08	This paper
		3.8	Nucleus	8.0 ± 0.1	Lester et al. 1990
		3.8	Nucleus	4.96	This paper
		6	Nucleus	5.9 ± 0.2	McLeod et al. 1993
		6	Nucleus	11.9	This paper
		2.7	K2[c]	3.89 ± 0.12	Greenhouse et al. 1991
		2.7	K2	3.10	This paper

[a] Positions calculated using offsets from K nucleus and assuming nuclear coordinates of Pipher et al. 1987.

[b] We estimate a 20% uncertainty in our photometry.

[c] Dietz et al. 1986.

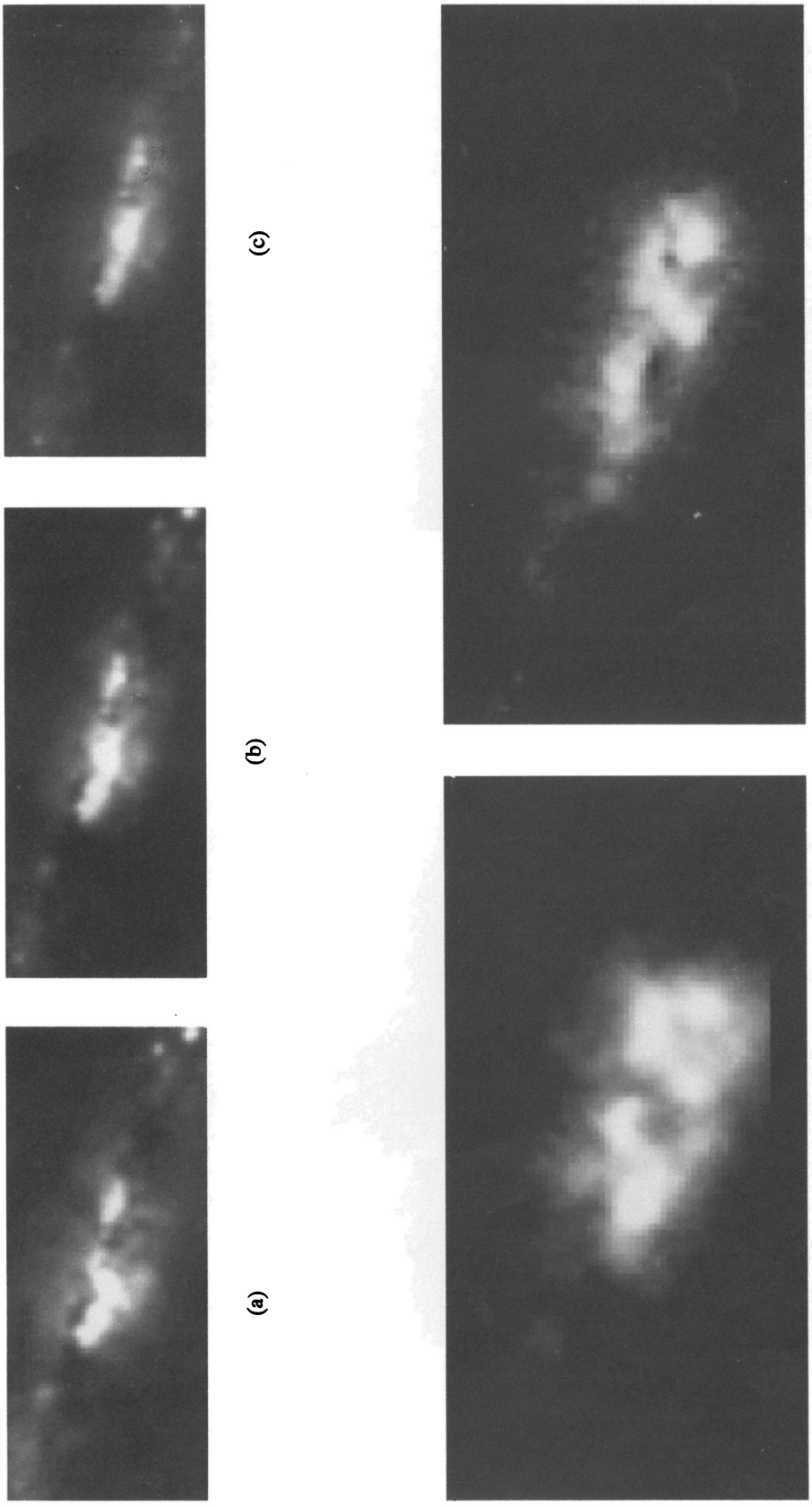

FIG. 2.—Gray-scale plots of the observed near-infrared broadband emission from the central kiloparsec region of M82. (*a*) *J*-band (1.23 μm) continuum image. (*b*) *H*-band (1.65 μm) continuum image. (*c*) *K*-band (2.23 μm) continuum image. (*d*) Brγ gray-scale. (*e*) Paβ gray-scale.

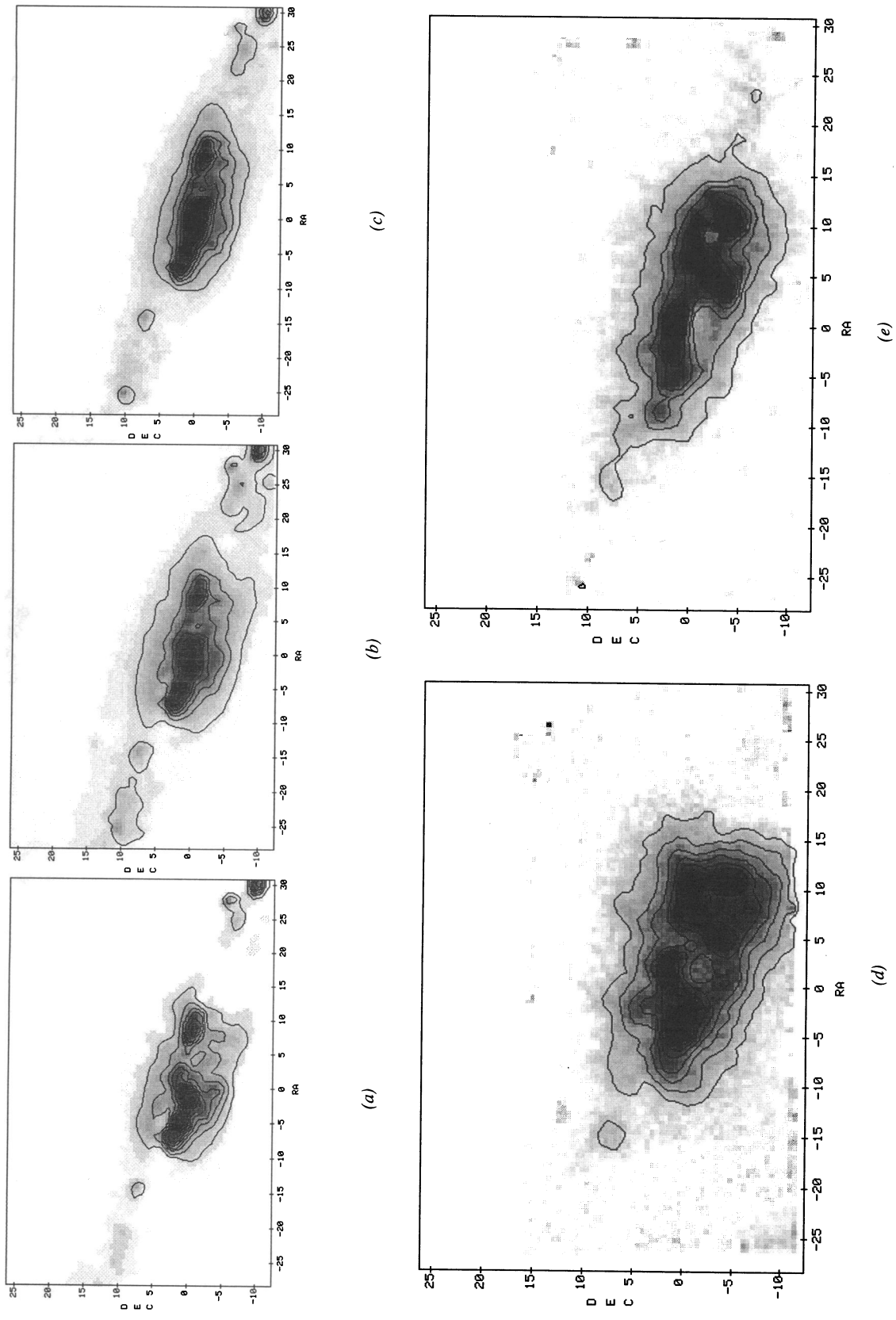

FIG. 1.—Gray-scale plots with contour overlays of the observed near-infrared broadband emission from the central kiloparsec region of M82. (*a*) *J*-band (1.23 μm) continuum image. The contour levels are from 2 to 12 mJy arcsec^{-2} in steps of 1 mJy arcsec^{-2}. (*b*) *H*-band (1.65 μm) continuum image contoured from 2 to 19 mJy arcsec^{-2} in steps of 2 mJy arcsec^{-2}. (*c*) *K*-band (2.23 μm) continuum image contoured from 3 to 21 mJy arcsec^{-2} in steps of 2 mJy arcsec^{-2}. (*d*) Paβ gray-scale with contour overlay. The contour levels are from 1.5×10^{-17} W m^{-2} arcsec^{-2} to 7.5×10^{-17} W m^{-2} arcsec^{-2} at intervals of 7.5×10^{-18} W m^{-2} arcsec^{-2}. (*e*) Brγ gray-scale with contour overlay. The contour levels are from 6×10^{-18} W m^{-2} arcsec^{-2} to 3×10^{-17} W m^{-2} arcsec^{-2}, at intervals of 4×10^{-18} W m^{-2} arcsec^{-2}. Right ascension and declination are in units of arcseconds, and the offsets are relative to the nuclear coordinates $\alpha(1950) = 9^h51^m43^s7$, $\delta(1950) = 69°55'00''3$ (Pipher et al. 1987). Note that the contours do not line up exactly with the corresponding gray-scale representations due to a software limitation.

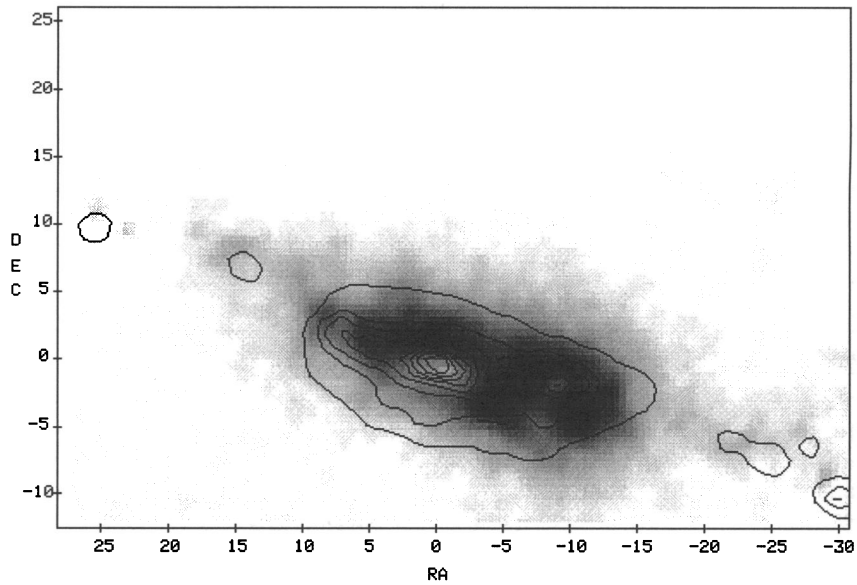

FIG. 3.—Brγ gray-scale with K contour overlay. Right ascension and declination are in units of arcseconds, and the offsets are relative to the coordinates $\alpha(1950) = 9^h51^m43^s.7$, $\delta(1950) = 69°55'00''.3$ (Pipher et al. 1987).

emission-line observations of these objects are less susceptible to the difficulties involved in emission-line observations of M82. Good agreement is found between our Fabry-Perot images of NGC 7027 and the single-aperture spectroscopic measurements by Geballe, Burton, & Isaacman (1991). We measure a flux of $88 \pm 10 \times 10^{-16}$ W m^{-2} in a 5″ synthetic aperture centered on NGC 7027, while Geballe et al. measure a flux of $80 \pm 5 \times 10^{-16}$ W m^{-2}. In addition, the difference between our spectrophotometry and the larger aperture measurements of NGC 7027 by Smith, Larson, & Fink (1981) are below 1%. Finally, our Brγ spectrophotometry is in close agreement with unpublished CVF images in this line that we obtained at Palomar in 1988, providing further confirmation of the accuracy of our photometry.

Table 3 is a summary of our 3.29 μm dust feature photometry in comparison with previous results. Our 3.29 μm photometry is in agreement with the measurements by Mitzutani, Suto, & Maihara (1989), Willner et al. (1977), and McLeod et al. (1993). The Tokunaga et al. (1991) result is substantially different from our own.

4. THE EXTINCTION TOWARD THE STARBURST REGION

4.1. *Extinction toward the Ionized Gas*

The high and nonuniform extinction toward the nuclear regions of M82 make reddening corrections essential for any quantitative model involving the stellar luminosity function. Extinction measurements have been carried out in the past

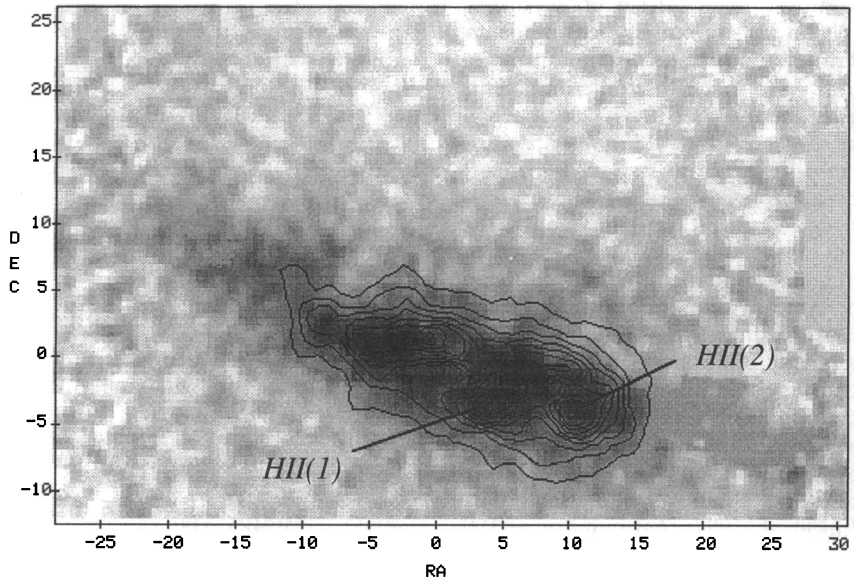

FIG. 4.—3.29 μm dust feature gray-scale displayed from 3×10^{-17} W m^{-2} arcsec^{-2} (*white*) to 4×10^{-16} W m^{-2} arcsec^{-2} (*black*) with the Brγ contour overlay. Right ascension and declination are in units of arcseconds, and the offsets are relative to the coordinates $\alpha(1950) = 9^h51^m43^s.7$, $\delta(1950) = 69°55'00''.3$ (Pipher et al. 1987).

TABLE 3

PHOTOMETRY FOR THE 3.291 μm FEATURE

Author	Aperture[a]	$F_{3.158}$ W cm^{-2} μm ($\times 10^{-18}$)	$F_{3.291}$ W cm^{-2} ($\times 10^{-18}$)	Instrument Resolution $\Delta\lambda/\lambda$	Equivalent Width (μm)
Tokunaga et al. 1991.....	2.″7	7.0	0.43	0.0007	0.051
McLeod et al. 1993.....	5.4	6.7	0.46	0.0125	0.067
Mitzutani et al. 1989.....	5.4 × 7.3	10.9	0.93	0.0083	0.059
Willner et al. 1977.....	30	70.0	6.95	0.02	0.087
This paper.....	2.7	3.9	0.16	0.0185	0.082
	5.4	9.6	0.63		
	7.2	14.6	1.09		
	30	63.1	8.21		

[a] Our photometry was done with circular apertures with specified diameter.

using a variety of methods. These methods have included the use of near-infrared broadband photometry, the depth of the 9.8 μm silicate feature, and combined optical/near-infrared recombination-line studies carried out at various spatial resolutions. Large discrepancies in the derived values of A_V have made the extinction toward the starburst region in M82 a controversial topic since it may imply a peculiar IMF. The uncertainty in the stellar population and the contribution to the J, H, and K emission from free-free and free-bound emission and the emission from transiently heated small particles has made the extinction derived from near-infrared broadband photometry potentially inaccurate. None of these methods approaches the accuracy that is possible with near-infrared hydrogen recombination line imaging, an established extinction law and favorable geometry. Given the configuration present in the starburst region of M82, this is a powerful and straightforward way of deriving the extinction *if* we assume that the molecular ring, as traced out by the CO and H I emission, dominates the extinction and can be treated like a foreground screen. For gas that is optically thick in the Lyman lines (case B recombination), the line ratios are only weakly dependent on temperature and electron density. Hydrogen recombination-line intensity ratios are used widely in the determination of extinction. However, past extinction studies of M82 have been based either on measurements at visible wavelengths or on large aperture near-infrared measurements. Extinction optical depth limitations and the nonuniformity of the dust distribution in M82 have made these measurements inconclusive in deriving the extinction.

The determination of the *reddening* toward heavily obscured ionized gas requires the measurement of at least two near-infrared hydrogen recombination lines. In order to determine the *extinction* toward the ionized gas at any wavelength, the extinction law appropriate to the observed region must be known. For Galactic H II regions with no nonthermal emission sources, observations of the optically thin radio continuum can be used to predict intrinsic near-infrared recombination-line fluxes, and a comparison of these predicted line strengths with those observed allow direct determination of the extinction law. Since the radio spectrum in M82 has large contributions from nonthermal processes in addition to thermal processes, this method will not work here. In our analysis, we have assumed purely foreground extinction and an extinction power law of $\tau_\lambda \propto \lambda^{-1.85}$ (Landini et al. 1984). Assuming $n_e = 100$ cm^{-3}, $T_e = 10{,}000$ K, and case B recombination, the intrinsic Paβ/Brγ line flux ratio is 5.84 (Hummer & Storey 1987). We attempted to test the validity of a power-law index of $\alpha = 1.85$ by using the dereddened Brγ image to generate a free-free continuum image at 3.3 mm, where thermal emission dominates. Synthetic aperture photometry was performed on this image and the results compared with the measurements by Carlstrom & Kronberg (1991). Since the actual emission from M82 at 3.3 mm has some nonthermal component as well as a component from dust, our Brγ-generated 3.3 mm photometry should be smaller than or roughly equal to the measurements by Carlstrom & Kronberg. The spectrum of M82 at the position of the source containing the largest observed 3.3 mm flux density, "mm(2)," is shown in Figure 5. Also shown is the free-free spectrum extrapolated from the extinction-corrected Brγ image (dereddened using three different extinction power-law indices (α). Extinction law A ($\alpha = 1.45$) results in an overestimate of the 3.3 mm flux density while extinction law C ($\alpha = 2.5$) results in a significant underestimate near 3.3 mm. At wavelengths greater than ~3 mm, the spectrum of M82 is expected

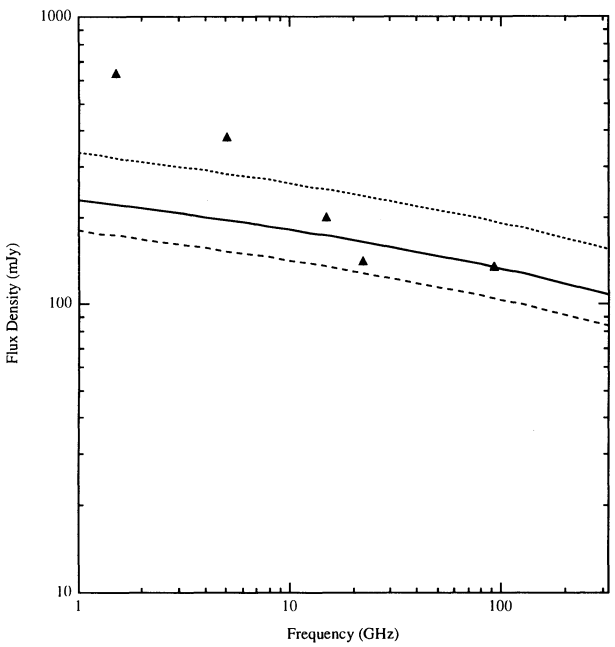

FIG. 5.—Spectrum of M82 in a 6″ aperture centered on the brightest 3.3 mm source ["mm(2)"] measured by Carlstrom & Kronberg (1991), at $\alpha(1950) = 9^h51^m41^s.5$, $\delta(1950) = 69°55'57''.5$. The filled triangles correspond to the data from Carlstrom & Kronberg at 1.5, 5, 15, 22, and 92 GHz. The three other lines correspond to the free-free spectrum calculated using our Brγ image, dereddened using three different power-law indices, α. The dotted line corresponds to extinction law A ($\alpha = 1.45$), the solid line to extinction law B ($\alpha = 1.85$), and the dashed line to extinction law C ($\alpha = 2.5$).

to be dominated by nonthermal emission from the numerous supernova remnants. Although the extinction power law cannot be determined very precisely from the data presented here, this analysis implies that the actual extinction law applicable to the starburst region in M82 does not deviate substantially from an $\alpha = 1.85$ power law.

Figure 6 shows our extinction map with a CO ($J = 1 \rightarrow 0$) and 6 cm overlay (Lo et al. 1987; Kronberg et al. 1985). This extinction image shows only those regions that are within the 2 σ level of the Brγ emission. The putative torus-shaped geometry of the CO emission is traced out well by our extinction map. The correspondence between the eastern CO lobe and the weaker central peak with regions of high extinction is particularly evident. The peak of the western CO lobe is just outside the 2 σ contour of our Brγ data. We can see that the prominent dust lanes are well resolved at a 1″ spatial resolution. It is quite remarkable that all the tracers of active star formation are contained between the two main CO lobes. The proliferation of bright radio sources along this ridge of extinction is also striking and shows that the starburst activity is confined to and ordered in the central regions of this galaxy. The dissimilarity of the inner structure from the overall chaotic apearance of M82 as seen in visible-light images accentuates the fact that the starburst phenomena is well confined to the central regions of this galaxy. The derived near-infrared extinction was converted to visual extinction by assuming $A_V = 10A_K$ (Draine 1989). Our derived value of A_V is in the range 2–12 mag, with the highest values near the nucleus at $A_V \sim 10$ mag.

The extinction inferred from the CO ($J = 1 \rightarrow 0$) emission can be compared with a similar region in our extinction map. Using the highest contour at the eastern CO peak and

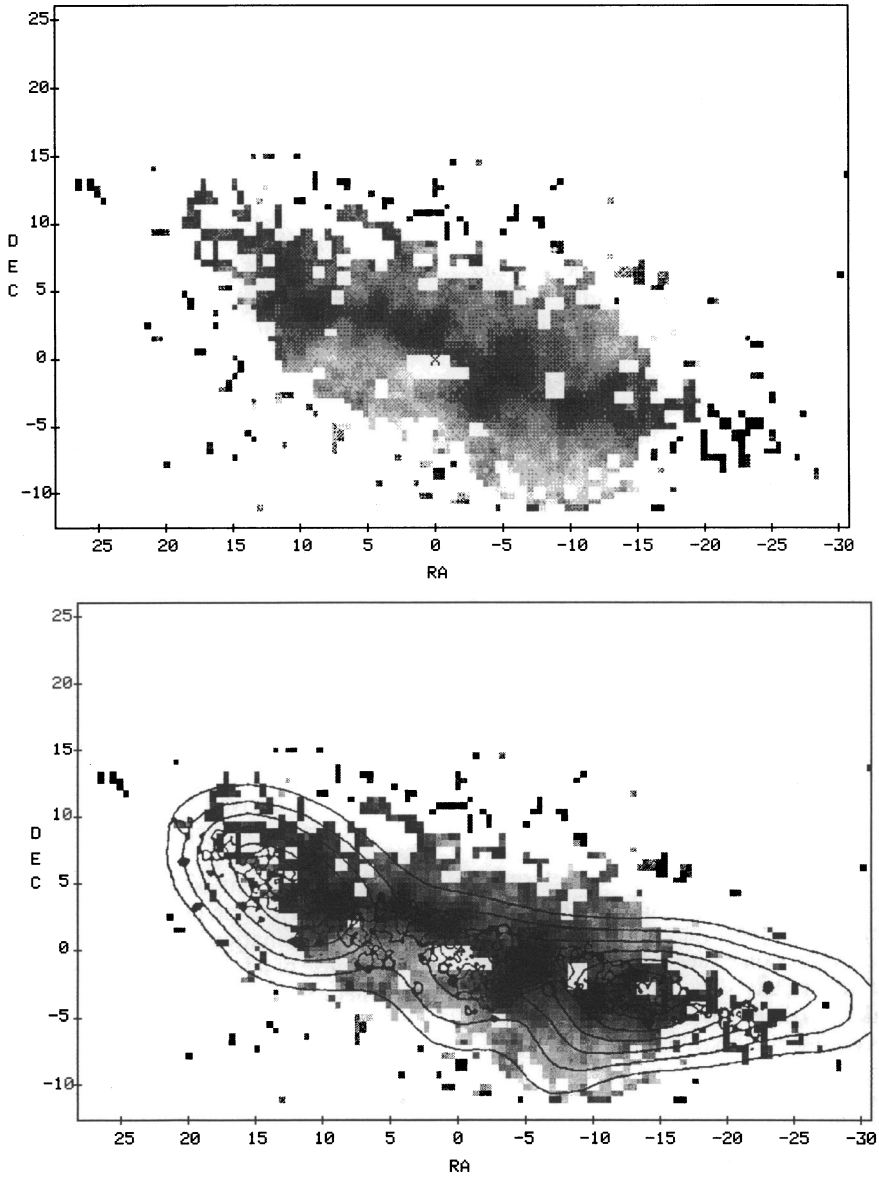

FIG. 6.—A_V derived from the recombination lines with and without the CO ($J = 1 \rightarrow 0$) contour overlay (Lo et al. 1987). The extinction map shows only those regions that are above the 2 σ level of the Brγ emission; thus within the starburst region, data are absent. Values are in the range 0–12 mag. Right ascension and declination are in units of arcseconds, and the offsets are relative to the nuclear coordinates $\alpha(1950) = 9^h51^m43^s.7$, $\delta(1950) = 69°55'00''.3$ (Pipher et al. 1987).

assuming a standard conversion factor of $N(H_2) = (3.0 \times 10^{20}$ cm^{-2})(I_{CO}/1 K km s^{-1}) (Young & Scoville 1991) applies, the inferred extinction is $A_K \sim 45$ [$N(H) = 1.89 \times 10^{22}$ cm^{-2} A_K; Draine 1989]. The corresponding region in our map has $A_K \sim 1$. As has often been asserted for M82, this suggests that the standard molecular gas conversion factor or the extinction-to-hydrogen nucleus column density conversion factor does not apply in M82. Recent results on other luminous infrared galaxies also show that this conversion factor is not the same as it is in the giant molecular clouds in our Galaxy (Shier, Rieke, & Rieke 1994). Using our extinction map, and the standard dust-to-gas ratio, the implied molecular gas conversion factor for M82 is $N(H_2) \sim (7 \times 10^{18}$ cm^{-2})(I_{CO}/1 K km s^{-1}).

We review other extinction results on M82 in comparison with our values. The large disparity in the results demonstrates the sensitivity of the derived extinction to wavelength and aperture size. Lester et al. (1990) find a Paβ/Brγ flux ratio in a 3".8 aperture centered on the nucleus which gives a visual extinction of 5.4 mag, assuming a $\tau_\lambda \propto \lambda^{-1.85}$ extinction law. As can be seen in Table 2, the Paβ flux deduced by Lester et al. is significantly higher than both our result and that by McLeod et al. (1993, hereafter MRRK). MRRK suggest that this difference in Paβ flux may be attributed to an error in the normalization of Lester's J-band continuum and possible pointing differences. In addition, Lester et al. scale the Brα measurements of Simon et al. (1977) in an 11" beam to their 3".8 aperture assuming that the Brα emission follows the continuum K emission. The derived visual extinction using this scaled Brα flux and their Brγ flux is 15 mag. From our Brγ and K-band data we have seen that the broad-band emission and ionized gas emission do not have the same distribution and therefore the scaling based on this assumption is incorrect. The K emission is more strongly peaked toward the nucleus than the Brγ emission, and the Lester et al. derived 15 mag of extinction would thus be an overestimate of the extinction in a 3".8 aperture centered about the nucleus. MRRK use their Paβ data, along with an assortment of previous optical and near-infrared recombination-line measurements, to derive the extinction in a small (6") and a large (30") region centered on the nucleus. For the small region, they scale the line fluxes to their beam size according to the 10 μm continuum emission. This scaling is more appropriate since the 10 μm emission follows the ionized gas emission, although care must be taken in applying a $S_\nu \propto \theta$ scale factor when the extinction is high and patchy and the wavelengths of interest differ substantially from 10 μm. Based on this scaling, the near-infrared recombination results in a 6" region are best fitted by a foreground screen extinction model with $A_V = 9$, consistent withour result.

Waller et al. (1992) have used the [S II] 9532/Hα flux ratio, and an adopted mean interstellar extinction law, to determine the extinction toward the M82 starburst complex. They find a visual extinction that ranges from 0 to 7 mag within the central kiloparsec, with the highest values on either side of the nucleus, along the major axis of the galaxy. The uncertainty in the excitation conditions makes this method less reliable than our near-infrared recombination line method. In addition, they use the Brγ/Hα ratio to generate an extinction map, yielding slightly smaller values for the extinction.

Larkin et al. (1994) generate an extinction map of the starburst region of M82 using similar spatial resolution near-infrared images. In the absence of a complete set of hydrogen recombination-line images, they fitted the observed colors at any given location to the emission from stellar photospheres, the emission from constant temperature dust, and the extinction from a foreground screen. Since we have a complete set of recombination lines, our extinction map is obtained directly from the line ratio, and this extinction map has been used to determine directly the components of the near-infrared emission (see § 5). Nonetheless, their extinction map looks very similar to ours, providing more support of the foreground screen treatment of the extinction toward the starburst region in M82.

It should be pointed out that all these methods for derivation of extinction have suffered either from the problems introduced by scaling larger aperture measurements to specific beam sizes, or the problems introduced by extinction optical depth limitations associated with shorter wavelength measurements, or the uncertainty in the method of extinction determination itself. This, coupled with the fact that both the extinction law used and the electron temperature adopted have lacked consistency in the literature, almost guarantees discrepacies between all of these methods. Since the dust lanes are resolved at our 1" spatial resolution, and since A_K is correlated with I_{CO}, the assumption of predominantly foreground extinction from a molecular torus surrounding the starburst region is confirmed. In addition, we have approximately confirmed the assumed $\tau_\lambda \propto \lambda^{-1.85}$ extinction law, making our near-infrared recombination line–derived extinction the most reliable derivation of the extinction to date toward the central starburst region of M82.

4.2. *Consistency of the Recombination Line–Derived Extinction with the Extinction Derived for the Extended Stellar Distribution*

The extended stellar distribution in M82 is expected to have an intrinsic infrared color consistent with normal unobscured galaxies with similar spectra. Such galaxies have intrinsic colors of $J-H \sim 0.85$ and $H-K \sim 0.28$ (Frogel et al. 1978). These colors correspond to a spectral type of M3, consistent with the observed CO bandhead strength in M82. If we assume these intrinsic colors, we can derive the extinction to check for consistency with the extinction derived from the Paβ/Brγ flux ratio. The $H-K$ color is less sensitive to variations in the stellar population and was thus chosen to determine the foreground screen extinction (assuming the same extinction law adopted for the recombination-line flux ratio) from the observed $H-K$ color. The resulting image of A_V is displayed in Figure 7. The bulk of the diffuse emission enclosed within the 2 σ contour of the Brγ image has A_V(gas) $- A_V(H-K) \sim 0$. Our $H-K$ derived extinction map is also well correlated with the CO map and agrees with the extinction map from Telesco et al. (1991).

The agreement between the extinction toward the *extended* stellar distribution derived from the observed $H-K$ color with our recombination-line extinction result provides confirmation of our use of a foreground screen model in our treatment of the extinction. Our extinction map derived from the Paβ/Brγ flux ratio can thus be used to deredden the emission from the stellar clusters in the starburst region of M82.

5. COMPONENTS OF THE CONTINUUM EMISSION IN THE NEAR-INFRARED AND THE STATE OF THE IONIZED GAS

In the absence of an active galactic nucleus (Seyfert nucleus or QSO), continuum emission from the nuclear regions of

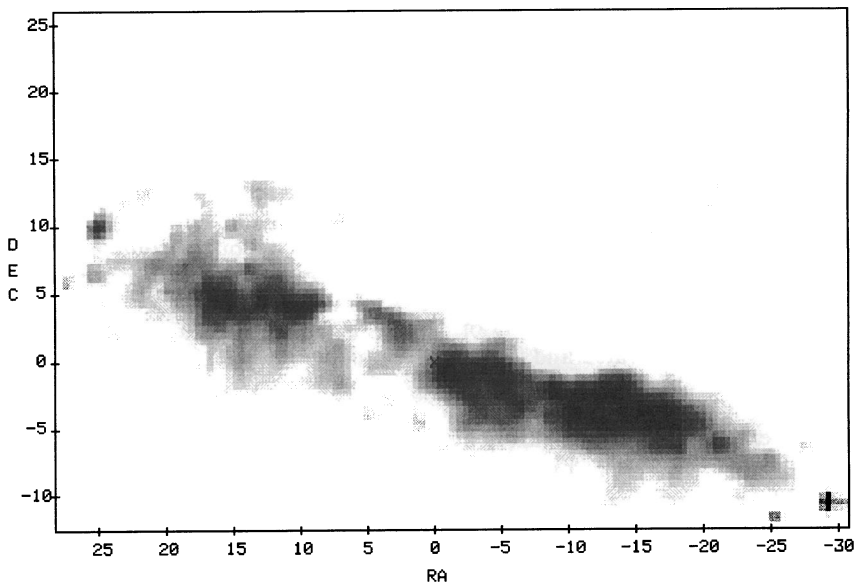

FIG. 7.—A_V derived from the $H-K$ color. Values are in the range 0–12 mag. Right ascension and declination are in units of arcseconds, and the offsets are relative to the nuclear coordinates $\alpha(1950) = 9^h51^m43^s.7$, $\delta(1950) = 69°55'00''.3$ (Pipher et al. 1987).

galaxies in the near-infrared bandpasses can be attributed primarily to stellar, free-free, free-bound, and dust emission. With the additional effects of reddening, near-infrared photometry alone does not allow us uniquely to separate these components. Near-infrared hydrogen recombination line images allow us to compute the contribution to the J, H, and K continuum from free-free and free-bound processes in addition to correcting for extinction. Assuming case B recombination with $n_e = 100$ cm^{-3} and $T_e = 10^4$ K, the contribution to the extinction-corrected continuum emission at each of the bandpasses is given by:

$$F(\lambda)(\text{mJy}) = C(\lambda)F_{\text{Br}\gamma}(\text{W m}^{-2}) ,$$

where $F_{\text{Br}\gamma}$ is the extinction-corrected Brγ flux, $C(J) = 6.22 \times 10^{12}$, $C(H) = 8.23 \times 10^{12}$, $C(K) = 1.02 \times 10^{13}$, and $C(3.3) = 1.27 \times 10^{13}$ for free-free emission and $C(J) = 1.47 \times 10^{13}$, $C(H) = 8.90 \times 10^{12}$, $C(K) = 1.11 \times 10^{13}$, and $C(3.3) = 5.08 \times 10^{12}$ for free-free-bound processes (W. J. Forrest, private communication). The relative contributions from these various processes are shown in Table 4.

An attempt was made to deduce the dust contribution to the continuum emission from the starburst region. The free-free and free-bound components were calculated as described above and subtracted from the dereddened J, H, K, and 3.3 μm emission. A blackbody fit was then applied to the residual J and H data and a color temperature was derived; this color temperature ranged from $T \simeq 3000$ to $T \simeq 5000$ K and is assumed to represent the stellar component of the near-infrared emission, containing a negligible contribution from either cool or "hot" dust emission. On the assumption that stars may be represented by blackbody spectra at near-infrared wavelengths and that dust emission makes a negligible contribution to the total J and H emission, the stellar emission at K is

$$F_K = \left(\frac{\nu_K}{\nu_J}\right)^3 \left[\frac{\exp(h\nu_J/kT) - 1}{\exp(h\nu_K/kT) - 1}\right] F_J .$$

This blackbody stellar component to the total K emission was also subtracted from the residual K emission. The result was taken to represent an upper limit to the dust contribution to the K-band emission. Table 4 shows the contribution to the K-band of this derived dust emission.

The same procedure was used to estimate the dust emission contributing to the 3.3 μm continuum. The estimated dust emission at 3.3 μm was used in conjunction with the estimated K dust emission and a color temperature was derived; this temperature was found to be $\lesssim$900–1000 K, characteristic of the continuum emission from transiently heated small dust particles (e.g., Sellgren 1981). It should be pointed out that this analysis involves a large number of assumptions and this attempt at calculating the dust emission should be viewed with caution. However, our analysis suggest that the "hot" and warm dust emission does not contribute appreciably to the

TABLE 4

CONTRIBUTIONS FROM NONSTELLAR PROCESSES TO THE CONTINUUM EMISSION

	CONTRIBUTION FROM FREE-FREE AND FREE-BOUND EMISSION (%)		CONTRIBUTION FROM HOT DUST (%)	
BANDPASS	Within 2 σ Brγ Contour	Compact K Sources	Within 2 σ Brγ Contour	Compact K Sources
3.3	0–25	0–10	0–30	0–15
K	0–20	0–8	0–20	0–8
H	0–14	0–5		
J	0–13	0–4		

total continuum emission in the near-infrared bandpasses, at least toward the compact broadband sources.

In addition, the recombination line strength can be used to estimate the contribution to the broad-band emission from young stars *if* we assume that all of the observed ionized gas is ionized by the UV photons provided by young stars. Assuming an intrinsic color of $J-K = -0.21$, $V-K = -0.93$, and $H-K = -0.05$, characteristic of O stars (Koornneef 1983), and adopting a distance of 3.2 Mpc to M82, the contribution to the broadband emission from O stars was computed and found to be a negligible constituent of the total continuum emission. The continuum emission from two-photon decay of the hydrogen $2^2S \rightarrow 1^2S$ state was also investigated and found to contribute insignificantly to the total continuum emission.

Various properties of the ionized gas can be derived using our recombination-line data. The extinction-corrected flux in a 3″.5 circular aperture centered on H II(2) (see Fig. 4) is 6.8×10^{-20} W m^{-2}. An emission measure of 1×10^6 cm^{-6} pc is required to produce this flux. Assuming a volume-filling fraction of unity, this implies an electron density of ~ 145 cm^{-3}. Assuming a spherical geometry, the mass of this region is $\sim 10^5$ $M_\odot$. The bright diffuse gas spread throughout the starburst region has a typical flux of $\sim 2 \times 10^{-17}$ W m^{-2} arcsec^{-2}. Using a 30″ × 8″ aperture, the corresponding emission measure is $\sim 10^5$ cm^{-6} pc and $n_e \sim 15$ cm^{-3}. The UV flux required to ionize H II(1) (see Fig. 4), for example, is $\sim 5 \times 10^{51}$ photons s^{-1}, equivalent to that produced by 200–300 O6 giants (Panagia 1973). This is a lower limit to the total UV flux since any dust would compete effectively with the gas for ionizing photons.

6. DISTRIBUTION OF THE 3.29 MICRON DUST FEATURE IN M82

The 3.29 μm feature is one member of the so-called family of unidentified dust features at 3.3, 6.2, 7.7, 8.6, and 11.3 μm, all of which are associated with interstellar dust. These features have been widely observed in planetary nebulae, H II regions, reflection nebulae, and starburst galaxies and are thought to be a result of a nonequilibrium process involving small grains (~ 10 Å) and UV photons. The 3.29 μm feature, observed in starburst galaxies and low-ionization nuclear emission-line regions (LINERS), has rarely been observed in pure active galactic nuclei (AGNs), suggesting that the presence of this feature is associated with star-formation activity in the nuclear regions of galaxies (Aitken & Roche 1985). Empirically, the ratio of the *total* far-infrared (FIR) luminosity to the 3.29 μm feature luminosity has been found to be roughly constant for a number of starburst galaxies (e.g., Dennefeld & Desert 1990; Mouri et al. 1990). The FIR luminosity in starbursts is generally thought to be due to thermal reradiation by ~ 0.1 μm sized dust heated primarily by UV photons produced by young stars, although the contribution by softer radiation from the older stellar population in heating the dust may be important in some cases (e.g., Thronson et al. 1990). If the source of the FIR luminosity is due primarily to young stars, the 3.29 μm feature can potentially serve as a probe of the regions of high star formation activity with the high spatial resolution that is possible in the near-infrared. Inherent in this hypothesis is the assumption that the grains that are responsible for the feature emission are associated closely with the larger FIR producing grains and that the abundance of these feature producing grains is constant in relation to the total dust composition. Given such a correlation, the 3.29 μm feature can potentially serve to obtain high spatial resolution information on the FIR luminosity, and thereby the regions of active star formation, provided the feature carriers are not destroyed in the radiation field surrounding the exciting stars. Since many starburst galaxies have high and nonuniform extinction affecting the emission even at 3.29 μm, accurate determinations of the 3.29 μm feature to total FIR luminosity ratio is dependent on high spatial resolution extinction information. Using the extinction map generated by our recombination-line images, the 3.29 μm feature image can be dereddened, allowing us to obtain a more accurate value for the ratio. We find $L_{\rm FIR}/L_{3.29} \approx 1340$ (using the dereddened 3.29 μm feature flux in a 30″ aperture and assuming $L_{\rm FIR} = 4.4 \times 10^{10}$ $L_\odot$; see Dennefeld & Desert 1990), substantially smaller than the value obtained using the uncorrected 3.29 μm feature flux (~ 1690). Since the 3.29 μm feature morphology is very similar to that at 12.4 μm which in turn is similar to the 30 μm emission (see Telesco et al. 1991 and Telesco & Gezari 1992), the 3.29 μm feature is most likely to be a good tracer of the FIR emission and hence the regions of recent star formation. If this ratio is to be used globally, accurate high spatial resolution extinction information toward starburst galaxies is essential.

If we are to use the 3.29 μm feature as a tracer of star formation locally within a galaxy, it is interesting to compare the 3.29 μm feature emission with the Brγ emission. In individual Galactic H II regions and planetary nebulae, the 3.29 μm feature emission is seen both immediately around and within the actual ionized region (e.g., Sellgren, Werner, & Dinerstein 1983; Woodward et al. 1989; Howard, Pipher, & Forrest 1994). This suggests that the 3.29 μm feature carriers can be excited by UV photons softer than the Lyman limit that penetrate to the outer neutral medium surrounding the ionized gas. Since the Brγ flux is related only to photons more energetic than the Lyman limit, while the 3.29 μm feature emission is also sensitive to less energetic photons, the 3.29 μm feature to Brγ flux ratio may be a crude indicator of the spectrum of the radiation field within the starburst region of M82. This extinction-corrected ratio is seen to vary radially from values greater than 35 near the dynamical center of the galaxy, to 10 in the adjacent H II region H II(1) (see Fig. 4), to six in H II(2). We take these differences to imply a variation in spectral type of the stellar clusters within the nuclear regions of M82. It has been proposed that the starburst activity propagates outward from the nucleus. If the H II regions within the starburst region farthest from the nucleus are powered by O stars, and those closer to the nucleus are powered by late O and B supergiants, the ratio can be qualitatively understood. Furthermore, the morphological difference in the bilobal 10 μm distribution that straddles the nucleus (see Telesco et al. 1991) and the recombination line emission from the rather symmetric centrally concentrated K-band emission is by itself highly suggestive of a radially dependent evolutionary effect. Additional support of this idea is offered by the strength of the photometric CO index in the central region of the galaxy. Lester et al. (1990) measure a CO index of 0.22 in a 3″.8 aperture centered on the nucleus. This is substantially larger than that seen in normal galactic nuclei (~ 0.15; Frogel et al. 1978). Although judging the luminosity class on the basis of the CO index is somewhat uncertain, an anomalously high CO index is suggestive of a nuclear stellar population of red supergiants, presumably remnants of the starburst. However, as pointed out by several authors, a high CO index can also be produced by a metal-enriched nuclear stellar population of giants that predated the starburst.

7. EXTINCTION-CORRECTED INFRARED COLORS AND LUMINOSITY

Most previous attempts to deredden the emission from the starburst region of M82 incorporated a single large-aperture extinction value. Based on the dust distribution discussed above, this is incorrect. Instead, we use the extinction map generated using the Paβ/Brγ flux ratio and the $\tau_\lambda \propto \lambda^{-1.85}$ extinction law to deredden the broadband images, generating extinction-corrected J, H, and K images. We then subtracted the free-free and free-bound components from the images and the remaining emission is assumed to represent the extinction-corrected stellar and dust emission (see § 5). The extinction-corrected K luminosity was calculated to compare with previously assumed values. Composite three-color images, before and after extinction corrections have been applied, are displayed in Figure 8 (Plate 23). The *observed* starburst region has an overall red appearance, while the corrected image is blue toward the compact broad-band sources, demonstrating that the observed colors in the starburst region of M82 are red generally as a result of the high extinction. Although all compact broadband sources are generally intrinsically blue (bluest regions have $H-K = -0.06$ and $J-K = -0.09$—characteristic of O stars), the region in the immediate vicinity of the dynamical center of the galaxy is intrinsically redder than the surrounding areas farther out. The red region immediately south of the nucleus in the uncorrected image is outside the 2 σ level of the Brγ emission and hence could not be dereddened; it is therefore unknown whether the region is red due to extinction or spectral character or both. The reddest regions in the corrected image have $H-K$ and $J-H$ colors of 0.40 and 0.60, respectively; these regions may still contain the emission from dust or there may be some internal extinction.

Our near-infrared extinction-corrected images will allow us to assess the true nature of the IMF of the starburst complex. The deciding factor which led Rieke et al. (1980) to infer a low-mass-deficient IMF was the extinction-corrected 2 μm luminosity. A large 2 μm luminosity, combined with the dynamical limits on the mass of the starburst complex, implies a large population of massive stars that would evolve to the supergiant phase within the timescale of the burst. For a 30″ aperture, we find that the observed K magnitude is 6.08 and the dereddened K magnitude is 5.51. At a distance of 3.2 Mpc, this corresponds to $M_K = -22.0$. For the same aperture, Rieke et al. (1980) find $M_K = -23.30$ using a homogeneous mixture model of dust and stars. This difference in magnitude corresponds to a factor of ~ 3 in the intrinsic K luminosity, a discrepancy that weakens the arguments for a low mass-deficient IMF for the starburst population. A quantitative analysis of the IMF of the starburst complex will be carried out in a future paper. In addition, using the integrated emission in a large aperture centered on the nucleus as a constraint in modeling a global IMF may prove to be an oversimplification. Our high spatial resolution observations will be used to deredden the individual stellar clusters within the starburst region, thereby allowing us to generate separate stellar cluster luminosity functions in our future paper.

8. CONCLUSIONS

High spatial resolution Brγ and Paβ Fabry-Perot, near-infrared broadband, and 3.29 μm narrow-band dust feature imaging observations of the central kiloparsec of M82 have been used to show the following:

1. The enhancements of the extinction-sensitive Paβ/Brγ flux ratio trace out the molecular lobes seen in CO, supporting our assumption of a dense, mainly foreground obscuring torus surrounding ionized gas and stars. The extinction derived from the Paβ/Brγ flux ratio ranges from $A_V \simeq 2$ to $A_V \simeq 12$ mag. The highest value near the nucleus is $A_V \simeq 10$ mag, substantially smaller than found in most previous studies at near-infrared wavelengths. The extinction was derived assuming a foreground screen for the obscuring material. A review of previous studies shows that extinction optical depth limitations and the nonuniformity of the dust distribution make past extinction determinations less reliable.

2. The extinction toward the extended near-infrared continuum emission derived from the recombination-line ratio is found to be largely consistent with the extinction derived from the assumption of a plausible intrinsic $H-K$ color. This offers additional support of our use of a foreground screen treatment of the extinction.

3. Our recombination line images were used to estimate separately the contribution to the near-infrared continuum bandpasses from free-free and free-bound emission as well as the emission from young stars. In addition, we have estimated the contribution from "hot" and warm dust. Our analysis suggests that these sources of emission do not contribute appreciably to the total continuum emission in the near-infrared bandpasses, at least toward the compact broadband sources; it can safely be assumed that this emission is dominated by starlight.

4. The 3.29 μm dust feature emission is seen to be correlated with the Bry emission. The morphology is even more similar to the 12.4 μm emission. The ratio of the extinction-corrected 3.29 μm dust feature flux to extinction-corrected Brγ flux is found to vary from 4.5 to 15 throughout most of the starburst region, with values greater than 35 near the dynamical center of the galaxy. This variation, along with other star formation diagnostics, suggests that the nucleus contains a later type stellar population and the starburst phenomena is propagating outward. The ratio of the total FIR luminosity to the dereddened 3.29 μm feature luminosity is found to be 1340 for M82, substantially smaller than the value obtained using the uncorrected 3.29 μm feature flux (~ 1690).

5. The extinction-corrected K-magnitude in a 30″ aperture centered on the nucleus is found to be $M_K = -22.0$. This is substantially fainter than previous values adopted, amounting to as much as a reduction of a factor of ~ 3 in the intrinsic K luminosity. The lower K-band luminosity will affect the inferred IMF of the starburst stellar population, resulting in an IMF for the starburst region that is much more like that of the solar neighborhood than has been previously assumed.

We would like to express our thanks to Mark Whitis, Kevin McFadden, and Jim Cole for their help in the Fabry-Perot instrument setup, software development, and telescope operation. We would also like to thank Eric Howard and Steve Solomon for their help with the observations, and the referee, W. Waller, for many useful suggestions. This work was supported in part by the Smithsonian Institution Scholarly Studies Program, NSF grants AST 89-57238, AST 93-57392, AST 91-16644, and AST 91-07769, National Geographic Society Grant 5077-93, the Office of Naval Research, and the Office of Research, University of Wyoming.

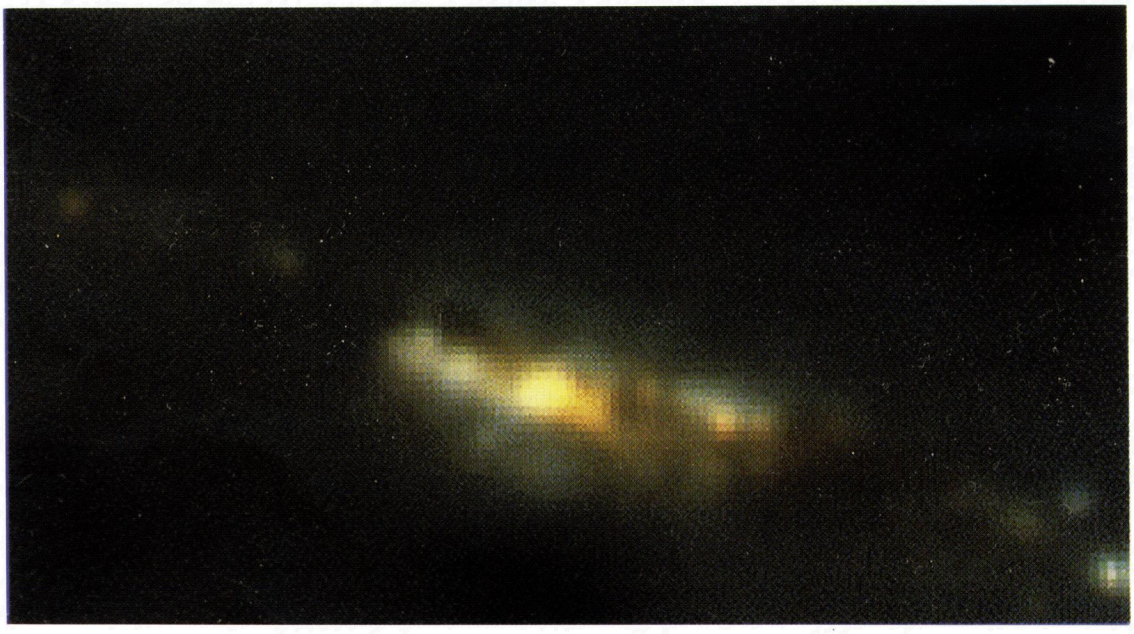

(a)

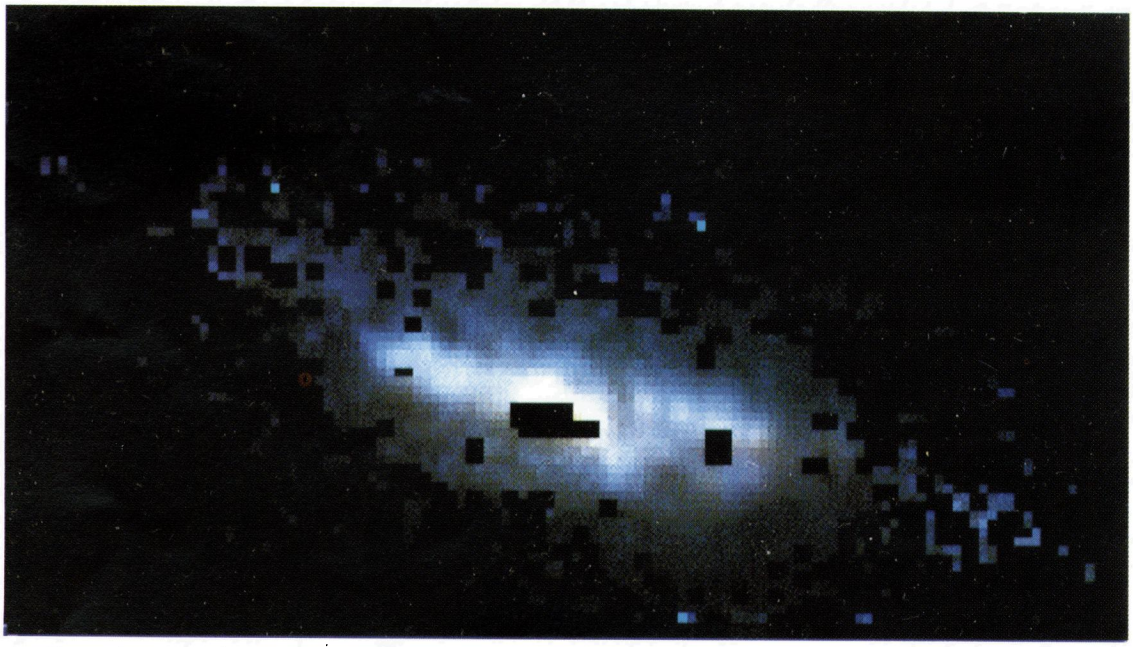

(b)

FIG. 8.—Three color image of the J (1.23 μm; blue), H (1.65 μm; green), and K (2.23 μm; red) emission before and after extinction corrections have been applied. The extinction map derived from the recombination-line ratio was used to deredden the broadband emission. Regions in the map that are below the 2 σ level of the Brγ image were clipped. (*a*) JHK image before extinction corrections have been applied. Within the 2 σ level of the Brγ map, the reddest regions have $H-K = 1.15$ mag and $J-H = 1.65$ mag, while the bluest regions have $H-K = 0.41$ mag and $J-H = 0.67$ mag. The peak K surface brightness is 11.5 magnitudes arcsec^{-2}. (*b*) JHK extinction-corrected image. Within the 2 σ level of the Brγ map, the reddest regions have $H-K = 0.41$ mag and $J-H = 0.60$ mag, while the bluest regions have $H-K = -0.06$ and $J-H = -0.09$. The peak K surface brightness is 10.2 mag arcsec^{-2}.

REFERENCES

Aitken, D. K., & Roche, P. F. 1985, MNRAS, 213, 77
Beck, S. C., Lacy, J. H., Baas, F., & Townes, C. H. 1978, ApJ, 231, 28
Carlstrom, J. E., & Kronberg, P. P. 1991, ApJ, 366, 422
Dennefeld, M., & Desert, F. X. 1990, A&A, 227, 379
Dietz, R. D., Smith, J., Hackwell, R. D., Gehrz, R. D., & Grasdalen, G. L. 1986, AJ, 91, 758
Doane, J. S., & Matthews, W. G. 1993, ApJ, 419, 573
Draine, B. T. 1989, in Infrared Spectroscopy in Astronomy, ed. B. H. Kaldeich (Noordwijk: ESTEC), 93
Elias, J. H., Frogel, J. A., Matthews, K., & Neugebauer, G. 1982, AJ, 87, 1029
Frogel, J. A., Persson, S. E., Aaronson, M., & Matthews, K. 1978, ApJ, 220, 75
Geballe, T. R., Burton, M. G., & Isaacman, R. 1991, MNRAS, 253, 75
Greenhouse, M. A., Woodward, C. E., Thronson, H. A., Rudy, R. J., Rossano, G. S., & Erwin, P. 1991, ApJ, 383, 164
Howard, E. M., Pipher, J. L., & Forrest, W. J. 1994, ApJ, 425, 707
Hummer, D. G., & Storey, P. J. 1987, MNRAS, 224, 801
Koornneef, J. 1983, A&A, 128, 84
Kronberg, P. P., Biermann, P., & Schwab, F. R. 1985, ApJ, 291, 69
Landini, M., Natta, A., Oliva, E., Salinari, P., & Moorwood, A. F. M. 1984, A&A, 134, 384
Larkin, J. E., Graham, J. R., Matthews, K., Soifer, B. T., Beckwith, S., Herbst, T. M., & Quillen, A. C. 1994, ApJ, 460, 159
Lester, D. F., Carr, J. S., Joy, M., & Gaffney, N. 1990, ApJ, 352, 544
Lo, K. Y., Cheung, K. W., Masson, C. R., Phillips, T. G., Scott, S. L., & Woody, D. P. 1987, ApJ, 312, 574
McLeod, K. K., Rieke, G. H., Rieke, M. J., & Kelley, D. M. 1993, ApJ, 412, 111 (MRRK)
Mitzutani, K., Suto, H., & Maihara, T. 1989, ApJ, 346, 675
Mouri, H., Kawara, K., Taniguchi, Y., & Nishida, M. 1990, ApJ, 356, L39
Panagia, N. 1973, AJ, 78, 929
Pipher, J. L., Moneti, A., Forrest, W. J., Woodward, C. E., & Shure, M. A. 1987, in Infrared Astronomy with Arrays, ed. C. G. Wynn-Williams & E. E. Becklin (Honolulu: Univ. Hawaii Press), 326
Rieke, G., Loken, K., Rieke, M., & Tamblyn, P. 1993, ApJ, 412, 99
Rieke, G. H., Lebofsky, M. J., Thompson, R. I., Low, F. J., & Tokunaga, A. T. 1980, ApJ, 238, 24
Sellgren, K. 1981, ApJ, 245, 138
Sellgren, K., Werner, M. W., & Dinerstein, H. L. 1983, ApJ, 271, L13
Shier, L. M., Rieke, M. J., & Rieke, G. H. 1994, ApJ, 433, L9
Simon, M., Simon, T., & Joyce, R. R. 1979, ApJ, 227, 64
Smith, H. A., Larson, H. P., & Fink, U. 1981, ApJ, 244, 835
Telesco, C. M., Campins, H., Joy, M., Dietz, K., & Decher, R. 1991, ApJ, 369, 135
Telesco, C. M., & Gezari, D. Y. 1992, ApJ, 395, 461
Thronson, H. A., Majewski, S., Descartes, L., & Hereld, M. 1990, ApJ, 364, 456
Tokunaga, A. T., Sellgren, K., Smith, R. G., Nagata, T., Sakata, A., & Nakada, Y. 1991, ApJ, 380, 452
Waller, W. H., Gurwell, M., & Tamura, M. 1992, AJ, 104, 63
Weliachew, L., Fomalont, E. B., & Greisen, E. W. 1984, A&A, 137, 335
Willner, S. P., Soifer, B. T., Russell, R. W., Joyce, R. R., & Gillett, F. C. 1977, ApJ, 271, L121
Woodward, C. E., Pipher, J. L., Shure, M., Forrest, W. J., & Sellgren, K. 1989, ApJ, 342, 860
Young, J. S., & Scoville, N. Z. 1991, ARA&A, 29, 581